Bottom-Up Tailoring of Plasmonic Nanopeapods Making Use of the Periodical Topography of Carbon Nanocoil Templates

Yong Qin, Ralf Vogelgesang, Moritz Eßlinger, Wilfried Sigle, Peter van Aken, Oussama Moutanabbir, and Mato Knez**

Au nanoparticle chains embedded in helical Al_2O_3 nanotubes ("nanopeapods") are synthesized by annealing carbon nanocoils coated with Au by sputtering and Al_2O_3 by atomic layer deposition. Regular spacing between nanoparticles with a sharp size distribution is achieved by fragmentation of the Au coating in agreement with the pitch of the nanocoils arising from three-dimensional periodical topography of the carbon nanocoil templates. A strong plasmonic resonance behavior of the fabricated nanopeapods manifests itself in confocal laser scanning microscopy by a clear polarization contrast at red wavelengths, which is absent in the blue. Numerical simulations confirm an incisive resonance enhancement for longitudinal polarization and suggest the nanopeapods as promising candidates for highly efficient, ultrathin waveguides. The waveguiding properties of the nanopeapods are investigated by electron energy-loss spectroscopy and energy-filtered TEM imaging.

1. Introduction

Linear metal nanoparticle chains exhibit unique physical properties compared with randomly distributed nanoparticles. In particular, their potential applications in waveguides, subwavelength imaging, high sensitivity Raman spectroscopy, nonlinear optics, and photoresponse sensors have attracted considerable interest.[1–7] Much effort has been devoted to develop various processes for the assembly of metal nanoparticles into ordered nanostructures. Currently, methods such as electron beam lithography,[8,9] template-based assembly,[10–12] block copolymer directed assembly,[13] dipole-directed assembly,[14] and applying external magnetic or electric fields,[15,16] have been used. While self-assembly routes enable metal nanoparticles to be incorporated into ordered structures, it is not straightforward to obtain controlled separation distances between nanoparticles. These nanoparticles are usually ordered in direct contact or separated by encapsulation materials.[17–19] Conventional electron beam lithography, focused ion beam, and scanning-probe nanomanipulation can lead to an excellent control over size, distance, and position of metal nanoparticles. However, the long time required limits severely the impact of these fundamentally serial processes. Another alternative method is the electrodeposition of striped metal nanowires followed by a selective etching or a solid-state reaction.[20,21] Depending on the pore size of the template and the length of the sacrificial metal sections, the particle size and spacing of the produced nanochains can be tuned. Recently, a cost-effective method to prepare nanoparticle chains based on the Rayleigh instability starting from metal nanowires (or narrow films) has received increasing attention.[22–29] However, this approach suffers from limited controllability because both the particle size and spacing are determined by the diameter of the starting nanowires.[30,31] Moreover, the substrates and surrounding environments will also impose considerable effects resulting in the deviation of the particle size and distance from the expected values with a broad distribution.

Here, we report the synthesis of Au nanoparticle chains embedded in helical Al_2O_3 nanotubes ("nanopeapods") based on

Prof. Y. Qin
Institute of Coal Chemistry
Chinese Academy of Sciences
030001, Taiyuan, P. R. China
E-mail: qinyong@sxicc.ac.cn
Dr. R. Vogelgesang, M. Eßlinger
Max Planck Institute for Solid State Research
70569 Stuttgart, Germany
Dr. W. Sigle, Prof. P. van Aken
Max Planck Institute for Intelligent Systems
70569 Stuttgart, Germany
Prof. O. Moutanabbir
Department of Engineering Physics
Ecole Polytechnique de Montreal
Montreal, C.P. 6079, Succ. Centre-Ville
Montreal, Quebec, H3C 3A7 Canada
Prof. M. Knez
CIC nanoGUNE Consolider
Tolosa Hiribidea 76, 20018 Donostia-San Sebastian
Spain Ikerbasque, Basque Foundation for Science
Alameda Urquijo 36-5, 48011 Bilbao, Spain
E-mail: m.knez@nanogune.eu

DOI: 10.1002/adfm.201201791

a guided Rayleigh instability. This is accomplished by annealing carbon nanocoils coated with sputtered Au and atomic layer deposited Al_2O_3. Carbon nanocoils are used as templates as well as sacrificial material for the creation of helical nanotubes and free volume simultaneously. The templates impose a spatial periodicity on the embedded Au nanoparticle chains that is closely reminiscent of peas in a pod. They have not only regular interparticle distances but also uniform particle sizes. The distances are determined by the coil pitches of the templates rather than the typical distance based on the Rayleigh instability equation. The waveguiding properties of the nanopeapods were investigated by confocal scanning laser microscopy, electron energy-loss spectroscopy and energy-filtered TEM imaging. Supporting numerical simulations also indicate that such plasmonic nanopeapods may be used as highly efficient, ultrathin waveguides.

2. Results and Discussion

The transmission electron microscopy (TEM) image in **Figure 1**a shows the morphology of the carbon nanocoils used in this study prepared as described previously.[32] The nanocoils have a diameter of about 100 nm. They are tightly coiled having a pitch close to the coil diameter. The as-prepared nanocoils show a uniform contrast before Au sputtering. However, the Au-coated nanocoil shows an enhanced contrast at one side instead of being uniform along the whole nanocoil as shown in Figure 1b. This is due to the fact that the Au coating, processed in a line-of-sight manner, does not completely cover the whole surface of the nanocoils. It can be inferred that Au covers about half the surface, as schematically displayed by the lower inset in Figure 1b. Figure 1c shows a scanning electron microscopy (SEM) image of the carbon nanocoils after Au sputtering and subsequent deposition of Al_2O_3 by atomic layer deposition (ALD). The dense stacking of the nanocoils resulted from the growth process. The helical morphology of the starting nanocoils is well-maintained after all processing steps. By applying 125 cycles of Al_2O_3 ALD, a conformal and uniform Al_2O_3 layer of about 12 nm thickness is deposited onto the Au-coated nanocoils, which is clearly visible from the brighter contrast as compared to the inner Au films (Figure 1d). The outer surface of the Al_2O_3 coating is perfectly smooth, as it is expected from ALD films.

By annealing the coated nanocoils in air at 650 °C the carbon cores are removed, resulting in helical Al_2O_3 nanotubes with encapsulated Au and free space. With extended annealing time the conversion of Au films into nanoparticles within the Al_2O_3 nanotubes takes place. Figure 1e shows an overview of the produced nanopeapods (also Supporting Information Figure S1).

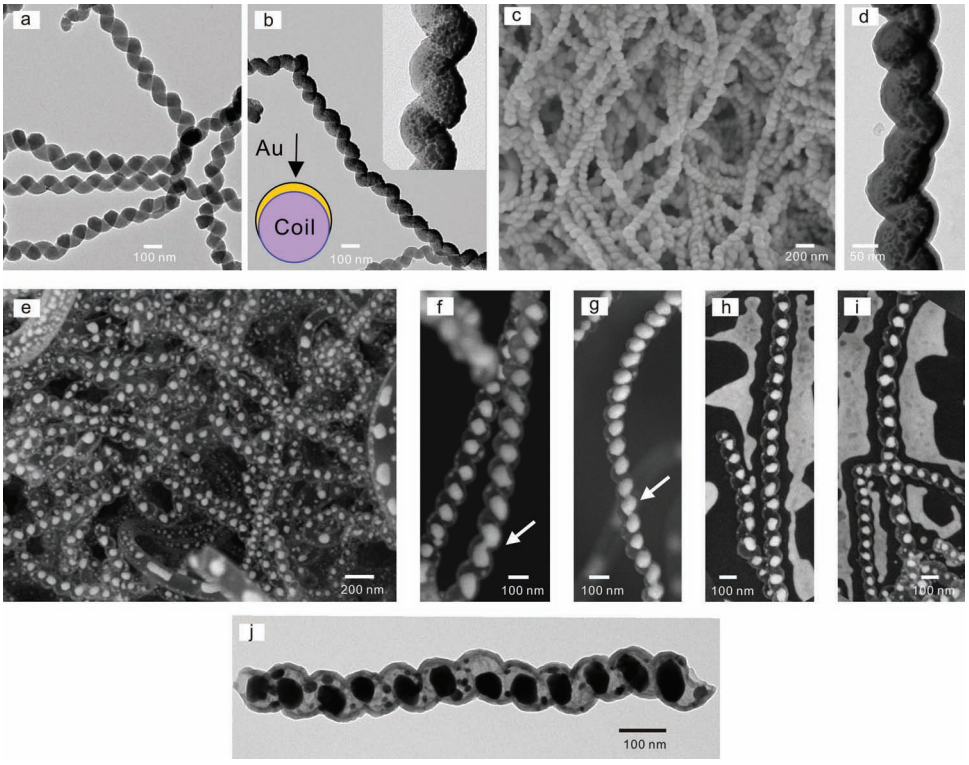

Figure 1. TEM and SEM images of carbon nanocoils templates and Au nanoparticle chains. a) TEM image of carbon nanocoils before Au sputtering. b) TEM image of carbon nanocoils after Au sputtering (40 nm thick). Insets: an image at higher magnification and a schematic of the cross-sectional shape of the Au coatings. Note that only one side is coated with Au. c,d) SEM and TEM images of carbon nanocoils after Au sputtering and deposition of Al_2O_3 by ALD (12 nm). e) SEM image of Au nanoparticle chains embedded in helical Al_2O_3 nanotubes obtained by annealing coated carbon nanocoils (shown in c,d) at 650 °C for 5 h. f,g) Close-up SEM images of suspended nanochains. h,i) Close-up SEM images of nanochains supported on Si wafers. j) TEM image of a single nanochain.

It can be observed that the Au films confined in the nanotubes undergo morphological changes to break up into nanoparticles with clear interparticle distances along the whole length of the nanotubes. The Au nanoparticles are clearly visible with a brighter contrast due to the much larger atomic mass of Au as compared to Al (Supporting Information Figure S2). In contrast, the thin shell of the Al_2O_3 nanotubes appears semi-transparent. Still the nanotubes well maintain the helical morphology of the starting nanocoil templates after annealing. Figure 1f–i are close-up SEM images of several suspended nanopeapods (Figure 1f,g) and of nanopeapods supported on Si substrates (Figure 1h,i). The embedded Au nanoparticles usually exhibit truncated shapes. Increased annealing temperatures induce a more spherical shape of the nanoparticles (Supporting Information Figure S3). We can clearly observe that these Au nanoparticles within a single nanotube reach a similar size and are generally regularly distributed. Interestingly, careful investigation shows that for every turn of the helical nanotubes there is always only one embedded Au nanoparticle, thus the distance between these nanoparticles is strictly controlled by the initial coil pitch of the template. This organization style is preserved even if the Al_2O_3 nanotube (or the initial nanocoils) considerably curve or change directions (Figure 1g). Figure 1i shows two nanopeapods of different diameters. It is obvious that both contain only one nanoparticle for every turn even if the diameters of the two nanotubes (90 and 140 nm, respectively) and also the size of these embedded nanoparticles (60 and 90 nm on average, respectively) are remarkably different. This reveals that this organization style has no relation to the difference in coil diameters and coil pitches of the starting nanocoil templates. Some incompletely fragmented sections are also observed (indicated by the arrows in Figure 1f,g), resulting from the insufficient annealing time or incomplete ripening and potentially revealing the intermediate state of the formation process of the nanochains. A representative TEM image of the nanopeapods is displayed in Figure 1j. This image most clearly reveals that the nanoparticles are periodically aligned within the Al_2O_3 nanotubes in accordance with the pitch of the nanotube with a relatively regular separation and that these nanoparticles are generally truncated in shape. Electron diffraction indicates that the Au nanoparticles have a polycrystalline structure (Supporting Information Figure S4). The TEM analysis is consistent with the SEM observations.

In order to investigate the process responsible of the morphological transformation of the Au films to Au nanoparticle chains, we perform stepwise annealing of coated nanocoils at various temperatures and times followed by SEM investigation at every stage. **Figure 2**a shows the SEM image of two coated nanocoils with coil diameters of 150 and 260 nm, respectively, supported on a Si substrate before annealing. Initially, a lower annealing temperature of 550 °C is applied. Figure 2b shows the morphology of the sample after annealing for 30 min. It can be easily observed that the coated nanocoil with a smaller diameter has undergone remarkable shape changes. Close analysis shows that some sections have been already fragmented into nearly spherical nanoparticles with a diameter of about 70 nm, while some sections show an important fluctuation of the diameter (ranging from 20 nm to 90 nm) along the

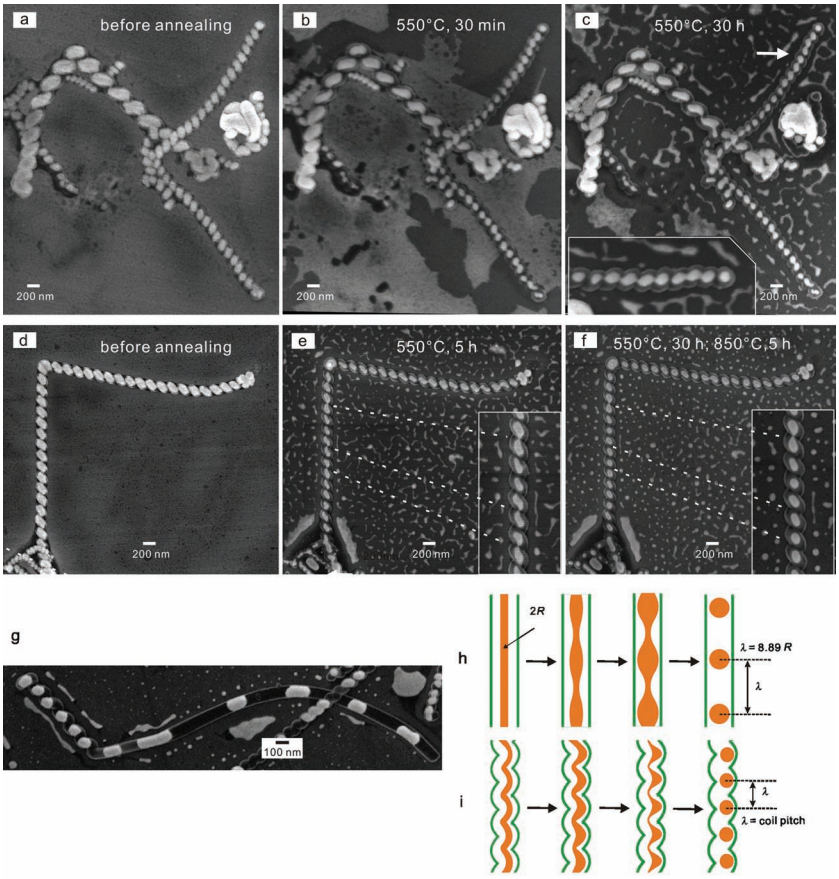

Figure 2. SEM images showing the transformation process of Au coatings by sequential annealing steps and a fragmentation mechanism of Au coatings in straight and helical nanotubes. a–c) Two coated nanocoils with different coil diameters and coil pitches. a) Before annealing. b) After annealing at 550 °C for 30 min. c) After annealing at 550 °C for 30 h. Inset in part (c) shows a magnified view of the section indicated by the arrow. d–f) A single coated nanocoil. d) Before annealing. e) After annealing at 550 °C for 5 h. f) After annealing at 550 °C for 30 h and then at 850 °C for 5 h. Insets in (e) and (f) show magnified views of the positions indicated by the dotted lines. After each annealing step, the samples are cooled down and taken out for SEM investigations. These coated coils are from the same sample and underwent the same heating process. Note that the Au coatings on the Si wafer also underwent changes after each annealing step. g) A nanoparticle chain confined in an Al_2O_3 nanotube containing both helical and straight sections. h) Schematic fragmentation mechanism of Au coatings confined in straight nanotubes. The Au coating breaks up into nanoparticles via gradually increased diameter undulation with separation λ determined by the diameter R of the starting nanowires in terms of a Rayleigh instability. i) Fragmentation mechanism of Au coatings confined in helical nanotubes produces nanoparticles with spacings determined by the coil pitch or turn wavelength of the helical nanotubes via diameter perturbation. The spacing is independent of the diameter of the starting nanowires. Here the Au coatings are considered as round nanowires.

longitudinal axis of the nanotube. Similarly, the coated nanocoil with a larger diameter also shows changes in morphology. The Au coating undergoes fragmentation according to the pitch of the confining nanotube. The produced nanoparticles show a long rod-like shape instead of a spherical shape and show an aggregating state due to the large particle diameter. The similarities of the behavior of Au coatings from the two coated nanocoils clearly reveal that the fragmentation style is not related to the coil diameter. The sample is further annealed at the same temperature extending the time to 5 h (not shown), and then to 30 h (Figure 2c), but no obvious change is observed indicating that further fragmentation is very slow at 550 °C. Figure 2d–f shows an analogous observation for another coated nanocoil from the same sample. After annealing at 550 °C for 30 min, no change can be observed (not shown), unlike the two coated nanocoils mentioned above. After heating for 5 h, the Au coating is mostly fragmented into separated particles except for some positions, which do not undergo thorough fragmentation (Figure 2e). Even upon further annealing at the same temperature (for 25 h), no change is observed in those positions (not shown). These factual observations prove that the further fragmentation is inhibited at this temperature. Consequently, a higher temperature is applied in the subsequent annealing step. After annealing at 850 °C for 5 h, the weakly connected positions fragment whilst the thickly connected positions did not (Figure 2f). The formed nanoparticles change to a more spherical shape. The shape changes observed by stepwise annealing clearly reveal the formation process of the nanoparticle chains. The Au coatings indeed fragment according to the turn wavelength of the helical nanotubes. The periodical 3D topography of the nanotubes plays an important role for the regular separation of the produced nanoparticles and also the uniformity of the particle size. The different fragmentation velocities for Au coatings within different nanotubes have plausibly resulted from to the differences in specific shapes, sizes and structures.

Figure 2g shows a nanotube containing both a straight section and a helical one, which is sometimes observed during the nanocoil template synthesis.[32] This figure clearly reveals the influence of the morphology of the nanotubes on the fragmentation manner of the Au coatings. We found that the particles confined in the straight section exhibit an elongated rodlike shape and have large particle sizes and separations. This is similar to previously reported results that metal nanowires break up into nanoparticle chains with their spacing defined by the Rayleigh instability equation by a fragmentation mechanism shown in Figure 2h.[24,27,29] However, in contrast, the separations between nanoparticles confined in the helical section are evenly spaced with a period given by the turn wavelength or coil pitch of the nanocoil. Apparently, this image most clearly reveals that it is the helical topography of the nanotubes that forces the Au coatings to break up into nanoparticles with regular separations according to the turn wavelength. Moreover, it also leads to the good uniformity in particle size. Therefore, based on the above analysis and the annealing stage-dependent SEM investigations, we propose a plausible mechanism to illustrate the formation process of the helical nanopeapods, as shown in Figure 2i. Upon heating in air to a high temperature, the carbon nanocoil templates are removed leading to the creation of the free volume. Subsequently undulations start on the surface of the Au coatings by self-diffusion and aggregate with an initial periodic perturbation already created due to the mimicked helical morphology. The undulation proceeds with a shorter wavelength through the imposition of the initial periodic perturbation, instead of the natural one on a flat substrate or in a straight nanotube. The driving force is still the reduction in surface area and total surface energy of the Au coatings.[30,31] It is possible that this is the fast route even if the reached energy state is not lower than the one according to the Raleigh instability shown in Figure 2h (nanoparticles with larger size having corresponding lower total surface energy). With extended heating time, the undulation grows and the subsequent morphological evolution always follows the periodical wavelength equal to the coil pitch of the helical nanotubes. Finally the thinner positions break leading to the formation of periodically distributed nanoparticles with regular distances and uniform and smaller particle sizes.

The effect of the Au film thickness on the product morphology is also investigated. **Figure 3**a–c show SEM images of nanocoils coated with 12 nm Au after annealing at 650 °C for 5 h. The Au coatings fail to transform into regularly distributed nanoparticle chains, but form irregularly distributed nanoparticles with diameters below 20 nm. They are randomly distributed on the inner surface of the nanotubes. The fragmentation of the Au coating behaves like the films on the Si wafers, which also produces small nanoparticles after annealing (Figure 3c). When the thickness of the Au coatings is increased to 25 nm, nanopeapods can be produced as shown in Figure 3d–f. The Au coatings break up basically according to the turn wavelength of the helical nanotubes dominantly producing larger nanoparticles. Some small nanoparticles, randomly scattered inside the nanotubes, are also observed. The Au coatings on the Si wafers obviously shrink to form nanoparticles with large sizes, unlike the thinner films shown in Figure 3c. When the thickness of the Au coating is further increased to 80 nm, the coatings break up into nanoparticles with a larger size as shown in Figure 3g,h. The distance of the nanoparticles reduces due to the increase of the particle sizes. Some Au coatings fail to fragment (Figure 3i) and display regular diameter undulation according to the turn wavelength of the helical nanotubes revealing a transition stage of the chain formation. This can be understood considering that the increase in thickness (corresponding to a diameter increase of starting nanowires) induces the necessity of a higher annealing temperature or a longer annealing time based on the Rayleigh instability.[24,29] From the above observation it can be derived that a critical thickness is necessary for the coatings to fragment and produce regular nanoparticle chains. When the coatings are initially very thin, they are, due to the applied sputtering method, actually discontinuous particulate films having randomly dispersed pinholes or many defects. Upon heating, aggregation occurs immediately at these sites and produces randomly distributed small particles.[33] This leads to the lack of a self-diffusion avenue for the Au atoms. Therefore, the coatings fail to form a large particle for every turn of the helical nanotube. With enough thickness of the coatings, annealing leads to breaking up into regular nanochains with a periodical distribution given by the turn wavelength and not correlated with the diameter of the starting nanocoil templates.

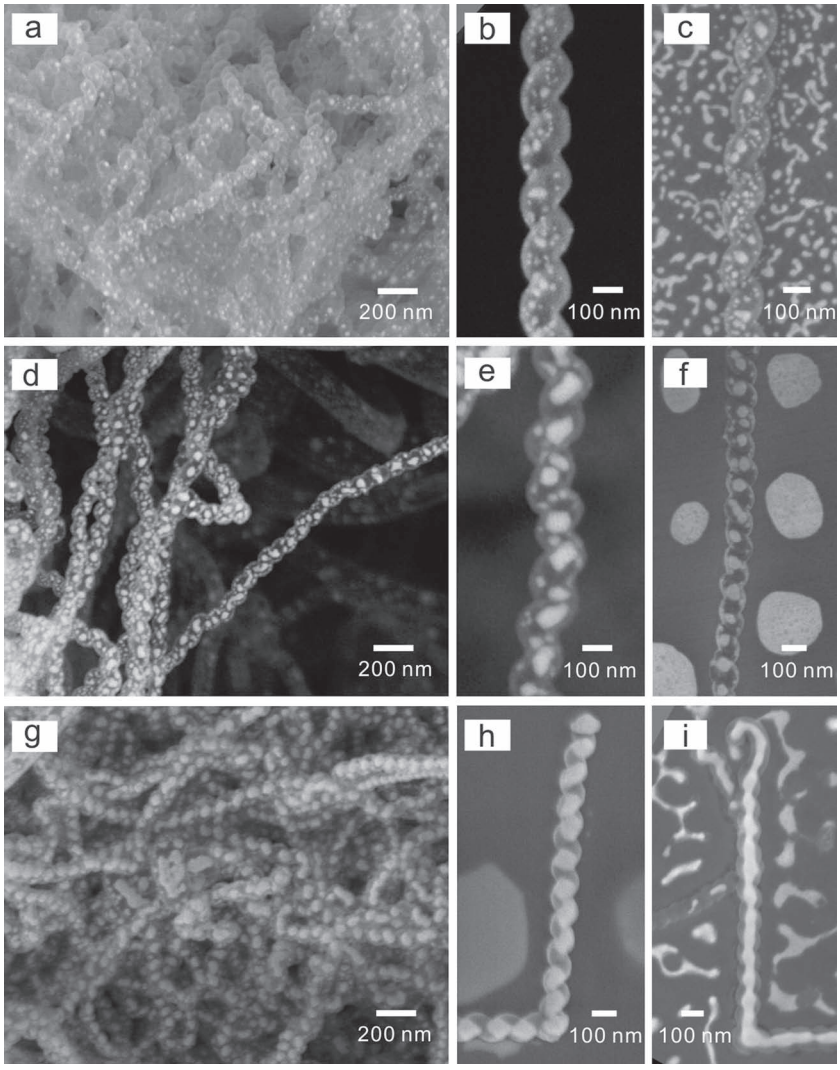

Figure 3. SEM images of carbon nanocoils coated with Au of different thickness by sputtering and ALD of Al_2O_3 (12 nm) after annealing at 650 °C for 5 h. a–c) 12 nm. d–f) 25 nm. g–i) 80 nm. b,e) Images of suspended sections at higher magnifications. c,f,h,i) Images of supported sections on Si substrates at higher magnification. Note that the Au films on the Si substrates also underwent transformation producing particle films with different features depending on thickness.

Metallic nanoparticle chains have been recognized as an important candidate class for optical nanodevices with functions such as transport and guiding, switching, or conversion of electromagnetic energy at subwavelength scales.[1,2,5,6,34–37] With this focus, we investigated optical properties of the Au/Al_2O_3 nanopeapods by confocal laser scanning microscopy. **Figure 4**a shows an SEM image of some nanopeapods on a Si substrate and their corresponding reflection images. By comparing the SEM image with the optical image using laser excitation at 458 nm, we can observe that all nanopeapods appear strikingly darker than their surroundings, including bare regions of the substrate. In contrast, the areas covered by Au in irregular shapes show brighter spots. A detailed comparison reveals that the darker contrast is not induced by the Al_2O_3 shells (Supporting Information Figure S5). As seen in the optical image, the particle-containing nanopeapods appear to significantly absorb the exciting radiation. It is well-known that metallic nanoparticles strongly interact with light, forming so-called surface plasmon polaritons, i.e., resonant collective oscillations of conduction electrons.[1,9,38–40] Even single particles exhibit dramatic enhancement of their electromagnetic near-fields. For sufficiently closely spaced particles, coupling can lead to energy shifts as well as further field confinement and enhancement.[35] To assess micro-spectroscopic properties, the nanopeapods are further studied with various laser excitation wavelengths (Figure 4a). When the laser excitation wavelengths are changed to 488 and 514 nm, the contrast reduces very slightly. Increasing the wavelength further to 543 nm and 633 nm, however, progressive changes are observed. The contrast weakens for the horizontally oriented nanopeapods, whereas it appears nearly steady in vertically aligned chains. The spectroscopic changes may be related to the resonant plasmonic behavior of isolated Au nanospheres. Indeed, Mie scattering theory expects a dipole resonance around 610 nm for individual Au sphere of diameter 80 nm, embedded in Al_2O_3, whose index of refraction is about 1.78 (Supporting Information Figure S6). However, the orientation dependence is unsuspected. Figure 4b displays a more systematic polarization study. For the two extreme wavelengths (458 nm and 633 nm) four different orientations of linear polarization are shown. Whereas the 458 nm image series reveals nearly isotropic behavior, in the 633 nm images always the nanopeapods oriented along the polarization direction exhibit a much reduced contrast, as indicated by the arrows.

To understand the spectroscopic behavior of long nanopeapods beyond the effective Mie scattering level, we perform numerical simulations of the scattering behavior of Au sphere chains embedded in dielectric cylinders of varying index of refraction. The sphere and cylinder diameters, period, and total length are calibrated to match the SEM image of Figure 4a. The simulation results reveal remarkable waveguiding abilities of plasmonic nanopeapods. When excited by a point dipole emitter situated at the "entrance", light is efficiently transmitted along the length of the nanopeapod and emitted at the "exit" end. As a measure of spectroscopic resonances, we show in **Figure 5** the electric field magnitude ratio of the scattered (i.e., transmitted by waveguide) to the exciting field (i.e, the bare dipole emission in the absence of any waveguide). Chains of plasmonic particles have been known to exhibit waveguiding for more than a decade,[1,2,34–37] including its close relation to resonances in the constituent particles. Correspondingly, the bare chain in vacuum ($\varepsilon = 1.0$) exhibits rather similar resonances around 550 nm for both longitudinal

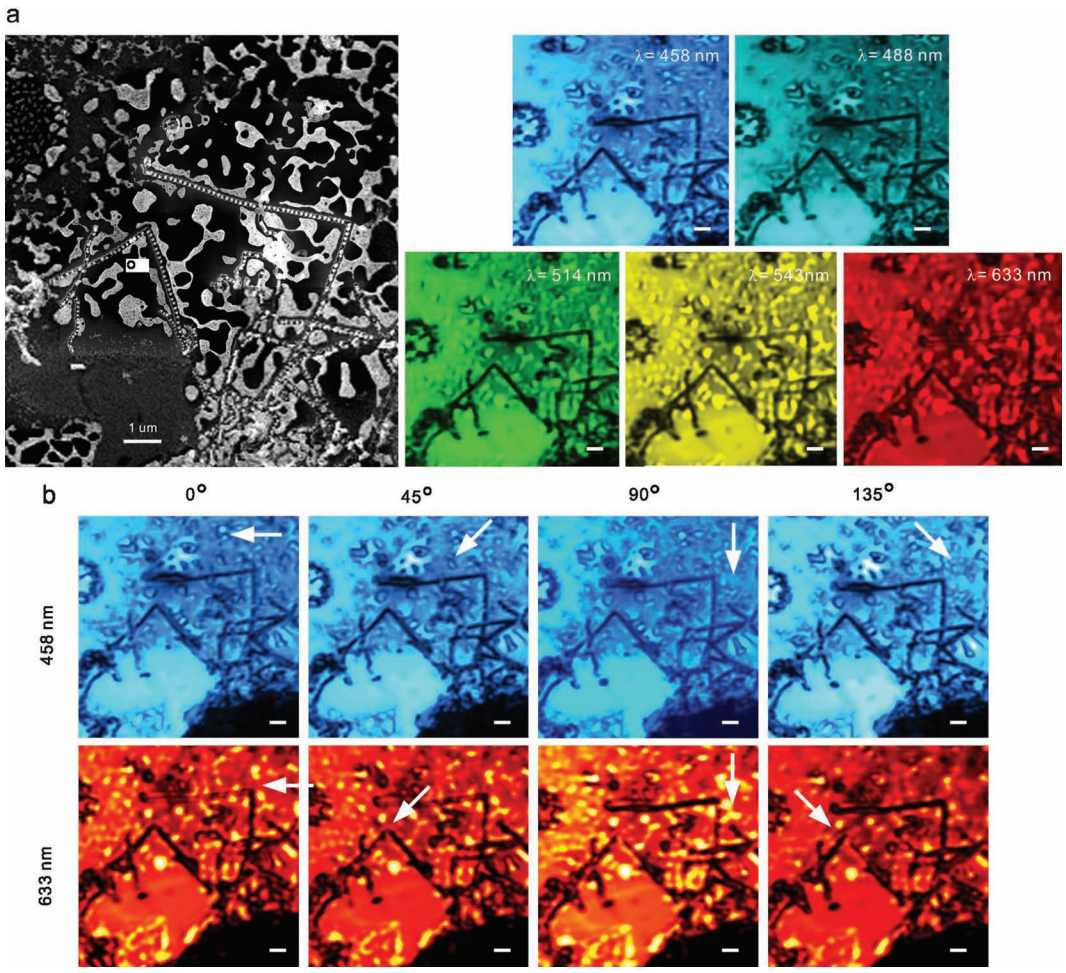

Figure 4. Spectroscopic property of Au nanoparticle chains. a) SEM image of embedded Au nanoparticle chains on a Si substrate and their corresponding false-color confocal microscopy reflectivity images obtained with laser excitation at 458, 488, 514, 543, and 633 nm, respectively. b) False-color confocal microscopy images of the Au nanoparticle chains shown in (a), recorded with 458 nm and 633 nm excitation radiation, which is linearly polarized along different orientations (0° corresponding to the horizontal image direction). Scale bars for all images are 500 nm.

and transverse excitation. Also, with an increase in the dielectric constant of the host medium, the pronounced red-shift of the resonance peak is not unexpected. The ensuing broadening, however, is much wider for the longitudinal than for the transverse polarization, and the difference in amplitude thrusts itself into attention. The transverse dipole emission is hardly boosted at all with a maximum enhancement of 6. But the longitudinal field becomes several hundred (up to 400) times stronger due to plasmonic nanopeapod waveguides, if their cladding material has a dielectric constant in excess of ≈ 4.0. Prominent examples are zirconia ($\varepsilon \approx 4.2$) and titania ($\varepsilon \approx 6.2$), which are available by ALD with well-established deposition processes. Also in the present case, for Al_2O_3 ($\varepsilon \approx 3.2$), the field enhancement is more than an order of magnitude stronger for longitudinal than for transverse polarization at 632 nm. This provides a strong indication that the observed loss of contrast in the optical reflection images taken at 632 nm (Figure 4) is due to resonantly enhanced scattering by plasmonic nanopeapods that are preferably excited by longitudinal polarization.

Further support to this conclusion is lent by experimental analysis using electron energy-loss spectroscopy (EELS) and energy-filtered TEM (EFTEM) imaging.[41] These techniques detect the energy loss suffered by a fast electron passing the structure. As can be seen from **Figure 6**b, pronounced peaks in the energy-loss spectra of a nanochain are observed at different energies, depending on the locations where spectra are recorded (also see Supporting Information Figure S7). Whereas inside a gold nanoparticle mainly the bulk plasmon contributes (around 2.45 eV, corresponding to radiation of 500 nm wavelength), between particles and especially between particles and the outside edge of the hull of nanopeapods another resonant mode manifests itself. Its significant red shift to a broad energy peak around 650 nm (corresponding to an energy loss of ≈1.85 eV) agrees well with the numerical prediction (Figure 5b). As the peak map in Figure 6c indicates, this mode extends over the entire nanopeapod, again in agreement with optical calculations (Supporting Information Figure S8).

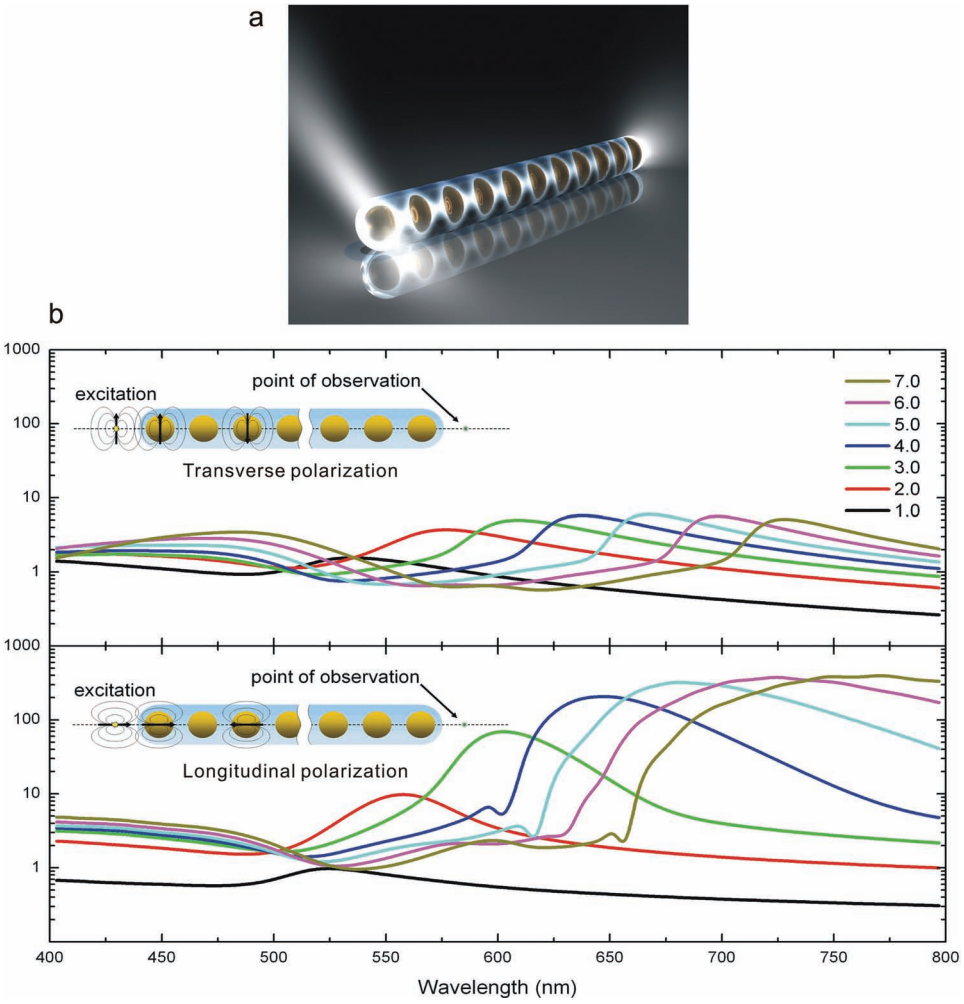

Figure 5. Simulated field transport along a plasmonic nanopeapod waveguide. a) Schematic of he simulated waveguide. It is similar to the one studied in Figure 4: Gold spheres of diameter 82 nm, embedded in a cylindrical dielectric rod of diameter 106 nm with a period of 149 nm. The waveguide is approximately 5.2 µm long, containing 35 spheres. b) Simulated field transport along the waveguide with different polarization directions of excitation. It is simulated for constant dielectric permittivity values ranging from 1.0 to 7.0, as indicated by the color scale legend. The case of Al_2O_3 corresponds to $\varepsilon \approx 3.2$. The energy-guiding efficiency is evaluated at the point of observation. First the electric field is computed in the presence of the waveguide and then without it. The ratio of field strength in the two cases is displayed. As optical power is proportional to the square of the electric field, these calculations predict a possible improvement in guided power by nearly five orders of magnitude.

3. Conclusion

In conclusion, a new method has been developed to prepare nanopeapods, i.e., Au nanoparticle chains encapsulated in nanotubes with a well-controlled spacing and sharp size distribution. This is achieved by annealing Au coated carbon nanocoils embedded in Al_2O_3 shells. The three-dimensional periodical morphology of the nanocoils plays an important role in the control of the regular spacing. The fragmentation process of the Au coatings has been investigated by stepwise annealing and SEM analysis. The helical topography of the nanocoil templates imposes a starting undulation for the Au coatings to fragment according to the turn period. The produced nanoparticle chains reveal strong surface plasmon resonance behavior as observed by confocal scanning laser microscopy. Longitudinal propagating waves are efficiently guided by plasmonic nanopeapods, which is verified by theoretical simulation. This explains the loss of absorptive contrast in optical reflection images as due to resonantly enhanced scattering. The waveguiding properties of the nanopeapods were investigated also with a confocal microscope revealing clear energy transfer along the nanopeapods with a red excitation laser. Further investigations were carried out by EELS and EFTEM imaging to reveal the waveguiding properties. Plasmonic nanopeapods have potential as extremely efficient waveguides, especially when subwavelength physical dimensions, broad band spectral performance, or mechanical stability are the issue. Compared to dispersed Au nanoparticles or nanoparticle films on a substrate, the encapsulated nanochains presented in this work have very good stability and reproducibility, which makes them good candidates

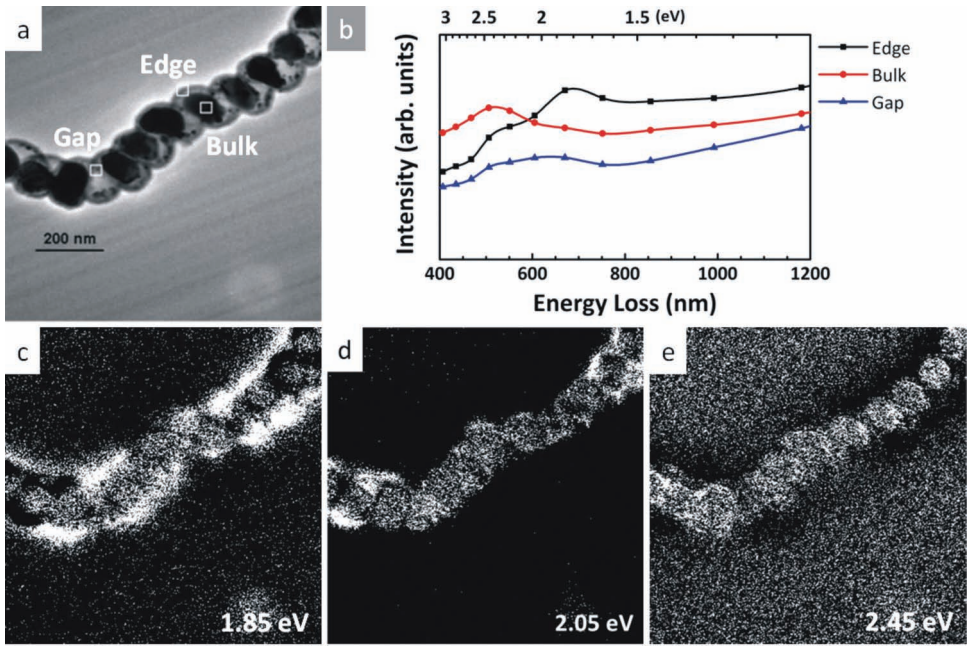

Figure 6. EFTEM and EELS analysis of a chain with more densily packed Au colloids. a) Bright-field TEM image. b) Electron energy-loss spectra acquired from the areas depicted in a. c–e) Maps showing the spatial distribution of peaks at 1.85 eV (c), 2.05 eV (d), and 2.45 eV (e).

for practical applications.[42] The freestanding nanochains can be manipulated and transferred and thus can be used as nanoprobes for optical waveguides or surface enhanced Raman scattering (Supporting Information Figure S9) yet maintaining activity. A long-range optical transport might be obtained with optimized structures and materials. Even a potential contrast between longitudinal and transverse mode could be beneficially used (Supporting Information Figure S8).

4. Experimental Section

Synthesis of Nanochains: The templates, the carbon nanocoils, were prepared by chemical vapor deposition inside a tube reactor using acetylene as a carbon source and copper nanoparticles as catalysts at 250 °C as reported previously. Prior to the coatings, the carbon nanocoils were dispersed in ethanol and then dropped onto a Si wafer with native oxide. After being air-dried, a Au layer with controlled thickness was deposited on the carbon nanocoils by ion sputtering. The thickness of the Au coatings was determined by cross-sectional analysis of Au films sputtered on a flat Si substrate. Subsequently the nanocoils were coated with Al_2O_3 by ALD. The Al_2O_3 film was deposited in a hot-wall flow-type ALD reactor (Picosun, Finland) at 150 °C. Trimethylaluminum ($Al(CH_3)_3$) and deionized H_2O were used as precursors. The growth rate for Al_2O_3 was about 1.0 Å per cycle. Finally, after the ALD process, the coated nanocoils were transferred to a furnace and annealed in air under ambient pressure at elevated temperatures to remove the carbon cores. The conversion of the Au films coated on the carbon nanocoils into nanoparticle chains was initiated during the annealing process.

Instruments: The morphology of templates and Au nanoparticle chains was investigated using the field emission SEM (FE-SEM, JEOL JSM 6701F) and the TEM (JEOL JEM 1010). For TEM analysis, the samples were dispersed in ethanol by ultrasonication for 10 s. Several drops of the suspension were pipetted onto a carbon-coated TEM Cu grid, which were allowed to dry at ambient temperature. Optical property of the Au nanoparticle chains was investigated with a Leica TCS SP2 confocal laser scanning microscope. EELS and EFTEM experiments were performed at the sub-electronvolt sub-angstrom microscope (SESAM Zeiss, Oberkochen, Germany) equipped with the MANDOLINE energy filter and a symmetric electrostatic Omega-type electron monochromator. Image processing was done by using Digital Micrograph (Gatan Inc., USA).

Theoretical Simulation Method: Simulations were done using the multiple multipole program (MMP) implemented in the open source platform OpenMaX.[43] This frequency domain boundary method expands fields in the volume using analytical solutions to the Maxwell equations and minimizes the boundary matching errors on the discretized two-dimensional interfaces separating domains. For the present case, the nanopeapod was considered perfectly rotationally symmetric, a cylinder with hemispherical caps, and the internal metallic spheres were periodically situated on the symmetry axis. As excitation source a point-dipole was assumed, located on the axis at the first periodic location outside the nanopeapod. The magnitude of the electric field at the corresponding location on the opposite side of the nanopeapod was evaluated as the ratio of the scattered field to the incident field. Taking advantage of the global rotational symmetry allowed further reduction of the problem to essentially one-dimension. After careful convergence checks, the scattering of plasmonic nanopeapods could be evaluated even for extreme aspect ratios of subwavelength width to multiple wavelength length (here more than 1:35).

Supporting Information

Supporting Information is available from the Wiley Online Library or from the author.

Acknowledgements

Y.Q., O.M. and M.K. acknowledge access to the infrastructure of the Max Planck Institute of Microstructure Physics, 06120 Halle, Germany used for a part of this work. Y. Q. acknowledges financial support from

National Natural Science Foundation of China (21173248) and the in-house project of SKLCC of China (Y1BWLI1991).

Received: July 1, 2012
Published online: August 8, 2012

[1] M. Quinten, A. Leitner, J. R. Krenn, F. R. Aussenegg, *Opt. Lett.* **1998**, *23*, 1331.
[2] S. A. Maier, P. G. Kik, H. A. Atwater, S. Meltzer, E. Harel, B. E. Koel, A. A. G. Requicha, *Nat. Mater.* **2003**, *2*, 229.
[3] V. F. Puntes, P. Gorostiza, D. M. Aruguete, N. G. Bastus, A. P. Alivisatos, *Nat. Mater.* **2004**, *3*, 263.
[4] A. Tao, P. Sinsermsuksakul, P. Yang, *Nat. Nanotechnol.* **2007**, *2*, 435.
[5] S. Kawata, A. Ono, P. Verma, *Nat. Photonics* **2008**, *2*, 438.
[6] S. Kawata, Y. Inouye, P. Verma, *Nat. Photonics* **2009**, *3*, 388.
[7] T. Yano, P. Verma, Y. Saito, T. Ichimura, S. Kawata, *Nat. Photonics* **2009**, *3*, 473.
[8] W. Gotschy, K. Vonmetz, A. Leitner, F. R. Aussenegg, *Opt. Lett.* **1996**, *21*, 1099.
[9] Q. H. Wei, K. H. Su, S. Durant, X. Zhang, *Nano Lett.* **2004**, *4*, 1067.
[10] Z. Y. Tang, N. A. Kotov, *Adv. Mater.* **2005**, *17*, 951.
[11] N. L. Rosi, C. S. Thaxton, C. A. Mirkin, *Angew. Chem. Int. Ed.* **2004**, *43*, 5500.
[12] G. D. Bachand, S. B. Rivera, A. K. Boal, J. Gaudioso, J. Liu, B. C. Bunker, *Nano Lett.* **2004**, *4*, 817.
[13] J. Chai, D. Wang, X. N. Fan, J. M. Buriak, *Nat. Nanotechnol.* **2007**, *2*, 500.
[14] M. Klokkenburg, C. Vonk, E. M. Claesson, J. D. Meeldijk, B. H. Erne, A. P. Philipse, *J. Am. Chem. Soc.* **2004**,*126*, 16706.
[15] J. C. Love, A. R. Urbach, M. G. Prentiss, G. M. Whitesides, *J. Am. Chem. Soc.* **2003**, *125*, 12696.
[16] H. L. Niu, Q. W. Chen, M. Ning, Y. S. Jia, X. J. Wang, *J. Phys. Chem. B* **2004**, *108*, 3996–3999.
[17] G. A. DeVries, M. Brunnbauer, Y. Hu, A. M. Jackson, B. Long, B. T. Neltner, O. Uzun, B. H. Wunsch, F. Stellacci, *Science* **2007**, *315*, 358.
[18] Y. Lu, Y. D. Yin, Z. Y. Li, Y. A. Xia, *Nano Lett.* **2002**, *2*, 785.
[19] S. L. Tripp, S. V. Pusztay, A. E. Ribbe, A. Wei, *J. Am. Chem. Soc.* **2002**, *124*, 7914.
[20] J. A. Sioss, C. D. Keating, *Nano Lett.* **2005**, *5*, 1779.
[21] L. F. Liu, W. Lee, R. Scholz, E. Pippel, U. Gosele, *Angew. Chem. Int. Ed.* **2008**, *47*, 7004.
[22] J. Lian, L. M. Wang, X. C. Sun, Q. K. Yu, R. C. Ewing, *Nano Lett.* **2006**, *6*, 1047.
[23] H. S. Shin, J. Yu, J. Y. Song, *Appl. Phys. Lett.* **2007**, *91*, 173106.
[24] M. E. Toimil-Molares, A. G. Balogh, T. W. Cornelius, R. Neumann, C. Trautmann, *Appl. Phys. Lett.* **2004**, *85*, 5337.
[25] C. Novo, P. Mulvaney, *Nano Lett.* **2007**, *7*, 520–524.
[26] H. Y. Peng, N. Wang, W. S. Shi, Y. F. Zhang, C. S. Lee, S. T. Lee, *J. Appl. Phys.* **2001**, *89*, 727.
[27] J. T. Chen, M. F. Zhang, T. P. Russell, *Nano Lett.* **2007**, *7*, 183.
[28] A. L. Giermann, C. V. Thompson, *Appl. Phys. Lett.* **2005**, *86*, 121903.
[29] Y. Qin, S. M. Lee, A. Pan, U. Gosele, M. Knez, *Nano Lett.* **2008**, *8*, 114.
[30] L. Rayleigh, *Proc. London Math. Soc.* **1878**, *10*, 4.
[31] F. A. Nichols, W. W. Mullins, *Trans. Metall. Soc. AIME* **1965**, *233*, 1840.
[32] Y. Qin, Z. K. Zhang, Z. L. Cui, *Carbon* **2004**, *42*, 1917.
[33] C. Hafner, OpenMaX, **2010**, http://openmax.ethz.ch/(accessed July, 2012).
[34] E. Jiran, C. V. Thompson, *Thin Solid Films* **1992**, *208*, 23.
[35] S. A. Maier, M. L. Brongersma, P. G. Kik, S. Meltzer, A. A. G. Requicha, H. A. Atwater, *Adv. Mater.* **2001**, *13*, 1501.
[36] M. L. Brongersma, J. W. Hartman, H. A. Atwater, *Phys. Rev. B* **2000**, *62*, R16356.
[37] S. A. Maier, P. G. Kik, H. A. Atwater, *Phys. Rev. B* **2003**, *67*, 205402.
[38] W. Nomura, M. Ohtsu, T. Yatsui, *Appl. Phys. Lett.* **2005**, *86*, 181108.
[39] U. Kreibig, M. Vollmer, *Optical Properties of Metal Clusters*, Springer, Berlin **1995**.
[40] R. Esteban, R. Vogelgesang, J. Dorfmüller, A. Dmitriev, C. Rockstuhl, C. Etrich, K. Kern, *Nano Lett.* **2008**, *8*, 3155.
[41] Q. B. Xu, J. M. Bao, F. Capasso, G. M. Whitesides, *Angew. Chem. Int. Ed.* **2006**, *45*, 3631.
[42] R. F. Egerton, *Electron Energy-Loss Spectroscopy in the Electron Microscope*, 2nd ed., Plenum Press, New York **1996**.
[43] J. F. Li, Y. F. Huang, Y. D. Zhi, L. Yang, S. B. Li, X. S. Zhou, F. R. Fan, W. Zhang, Z. Y. Zhou, D. Y Wu, B. Ren, Z. L. Wang, Z. Q. Tian, *Nature* **2010**, *464*, 392.